Journal of Trace Elements in Medicine and Biology 52 (2019) 232–238

Contents lists available at ScienceDirect

Journal of Trace Elements in Medicine and Biology

journal homepage: www.elsevier.com/locate/jtemb

Biochemistry

Desferrioxamine-caffeine shows improved efficacy in chelating iron and depleting cancer stem cells

Bin Li[a,b,1], Breno Pannia Espósito[c,1], Shunhao Wang[b,d], Jie Zhang[b,d], Ming Xu[b,d], Shuping Zhang[e], Zhihong Zhang[a,**], Sijin Liu[b,d,*]

[a] Department of Urology, Tianjin Institute of Urology, The Second Hospital, Tianjin Medical University, Tianjin 300211, China
[b] State Key Laboratory of Environmental Chemistry and Ecotoxicology, Research Center for Eco-Environmental Sciences, Chinese Academy of Sciences, Beijing 100085, China
[c] Department of Fundamental Chemistry, Institute of Chemistry, University of São Paulo, São Paulo 05508-000, Brazil
[d] University of Chinese Academy of Sciences, Beijing 100049, China
[e] Institute for Medical Engineering and Science, Massachusetts Institute of Technology, Cambridge, MA 02139, USA

ARTICLE INFO

Keywords:
Iron chelation
DFCAF
CSCs
EMT
Cancer therapeutics

ABSTRACT

Iron chelation has already been proposed to be a feasible strategy for cancer therapeutics in that reinforced iron demand is demonstrated in cancer cells, and quite a few iron chelators have been developed for this purpose. Desferrioxamine (DFO), an iron chelator approved by the U.S. Food and Drug Administration (FDA), has been extensively examined to remove extra iron. However, DFO has been found to harbor limited efficacies in combating cancer cells due to poor cellular permeability. In the current study, we synthesized the DFO derivative, named as desferrioxamine-caffeine dimer (DFCAF) by linking DFO to caffeine with high purity and excellent stability. Our data showed that DFCAF displayed greater cellular permeability to chelate intracellular iron in 4T1 breast cancer cells than DFO, posing more inhibition on cell growth and cellular motility/invasion. Importantly, DFCAF was uncovered to remarkably deplete cancer stem cells (CSCs), as characterized by the remarkable decrease of the $CD44^{+/high}/CD24^{-/low}$ and $ALDH^{+/high}$ subpopulation. In parallel, DFCAF was also found to greatly reverse epithelial–mesenchymal transition (EMT), suggesting the potential application to restrain tumor progression and metastasis. Collectively, these data unveiled the improved efficacy to target cancer cells and to deplete CSCs, thus opening a new path for better cancer therapeutics through iron chelation.

1. Introduction

Iron (Fe) is essentially involved in diverse cellular processes, including energy production, enzyme-mediated functions, DNA synthesis and electron transfer [1,2]. However, the iron level has to be concertedly governed to maintain fine-tuned iron recycling, whereas disordered iron metabolism would result in various diseases including cancers [3,4]. For example, reinforced iron supply has been uncovered to enhance tumor progression [5,6]. To this end, iron chelation has been examined to restrain tumor growth by starving tumor cells from iron as an essential nutrient [7,8]. Thus far, a few iron chelators have been tested for the purpose of tumor treatment. Of them, deferoxamine (DFO) represents a family of widely used iron chelators to remove excess iron in many diseases with iron overload [9], and further to treat cancers [10,11]. However, the current DFO family members still suffer from a few drawbacks, such as limited cellular permeability, fast clearance and low efficacy in targeting cancer cells [12]. Under this context, new DFO derivatives are sought for better performance in targeting cancer cells.

Cancer stem cells (CSCs) represent a tiny subpopulation of cancer cells in the tumor, and harbor some unique characteristics, *e.g.* the capabilities in self-renewal and generating heterogenic cancer cell populations [13]. Importantly, CSCs are thought to be the likely source of tumor initiation, progression, drug resistance, metastasis and recurrence [14,15]. Thus, targeting CSCs is becoming a promising strategy to treat cancers, especially for advanced cancers [16]. CSCs are rapidly dividing cells, requiring sufficient iron supply for cell growth and proliferation [17]. Given this property, we hypothesize that CSCs could

* Corresponding author at: Department of Urology, Tianjin Institute of Urology, The Second Hospital, Tianjin Medical University, Tianjin 300211, China.
** Corresponding author.
E-mail addresses: drzhangzhihong@163.com (Z. Zhang), sjliu@rcees.ac.cn (S. Liu).
[1] These authors equally contributed to this work.

https://doi.org/10.1016/j.jtemb.2019.01.004
Received 17 September 2018; Received in revised form 4 December 2018; Accepted 7 January 2019

be targeted through iron chelation.

In the current study, we aimed to synthesize the DFO derivative and target the CSCs in breast cancer. We first synthesized the desferrioxamine-caffeine (DFCAF) by linking DFO to caffeine, a very safe and highly biologically penetrable molecule, as we established previously [12]. Our combined data uncovered the improved efficacy of DFCAF in chelating iron and depleting CSCs. This study would open a new path for cancer therapeutics through enhanced iron chelation.

2. Materials and methods

2.1. DFCAF synthesis and characterization

DFCAF synthesis was carried out according to our previous protocols [12], based on the conjugation of DFO with theophylline-7-acetic acid (T7A) assisted by *N*-(3-dimethylaminopropyl)-*N′*-ethylcarbodiimide to form a covalent amide bond between the siderophore and the caffeine moiety. DFCAF was obtained as a beige powder, being insoluble in water and slightly soluble (up to 2 mM) in DMSO. Elemental analysis ($C_{34}H_{56}N_{10}O_{11}$·1.5 H_2O): calculated (%), C, 50.6; H, 7.36; N, 17.3. Found (%): C, 50.7; H, 7.18; N, 17.1. Moreover, 300 MHz representative 1H-NMR spectra were determined for DFCAF dissolved in DMSO-d6 (Agilent INOVA). As shown in Fig. S1, ^{1}H NMR (300 MHz, DMSO-d_6) δ_H (ppm): 1.14–1.29 (m, 6 H), 1.29–1.58 (m, 12 H), 1.95 (s, 3 H), 2.21–2.31 (m, 4 H), 2.54–2.61 (m, 4 H), 2.95–3.10 (m, 6 H), 3.20 (s, 3 H), 3.41–3.50 (m merged with s, 9 H), 4.93 (s, 2 H), 7.77 (t, 2H, J = 6 Hz), 7.99 (s, 1 H), 8.18 (t, 1H, J = 6 Hz, corresponding to the newly formed amide bond between T7A and DFO), 9.61 (broad s, 2 H), and 9.65 (broad s, 1 H). Effective coupling of the caffeine moiety to DFO was detected by the appearance of $\nu_{C=O}$ (xanthine ring) at 1667 and 1706 cm^{-1}, which is absent in DFO, and by the disappearance of the carboxylic stretch of T7A at 688 cm^{-1} with Perkin-Elmer Frontier (Fig. S2). LCI/MS for DFCAF ($C_{34}H_{56}N_{10}O_{11}$; 780.8 g/mol; Fig. S3): Charge 1+, experimental Mw = 781.5 g/mol; Charge 2+, experimental Mw = 391.2 g/mol, as described previously [12]. The purity of this compound is > 95%. After dissolving in DMSO and being saved at −20 °C for more than a year, DFCAF still revealed a potent efficacy in iron chelation, demonstrating its excellent stability.

2.2. Cell culture

Murine breast cancer cell line 4T1 was obtained from the American Type Culture Collection (Manassas, VA, USA), and 4T1 cells were cultured in phenol red-free RPMI-1640 medium (Gibco BRL Life Technologies Inc, USA) supplemented with 10% fetal bovine serum (FBS) and 1% penicillin/streptomycin (Invitrogen) in a humidified incubator with 5% CO_2 at 37 °C.

2.3. Measurement of intracellular iron

After treatment with DFO (Sigma-Aldrich) and DFCAF at 20 μM for 24 h, cells were washed with PBS and then incubated with Calcein-AM (ATT Bioquest, Inc.) at 1.0 μM, a cell-permeant form of calcein, for 20 min. Thereafter, cells were washed with PBS twice, and iron binding efficacy was determined through flow cytometry analysis.

2.4. Western blot analysis

Western blotting was carried out following the standard procedure, as previously described [18]. Antibodies used here were described in Supplementary Table 1. β-actin was used as a loading control for normalization.

2.5. CCK8 cell viability assay

Cell viability was assessed through the CCK8 assay following the manufacturer's protocol (Solarbio Science & Technology Co., Ltd., Beijing, China). In brief, 5000 cells were inoculated into 96-well plates, and cells were then subjected to different concentration of DFO and DFCAF at 2.5, 5, 10 and 20 μM for 24 h. Cell viability was then determined with the provided reagents.

2.6. Mammosphere formation assay

Mmmospheres originated from 4T1 cells were cultured in 6-well ultra-low attachment plates (Corning Costar Inc, Corning, NY, USA) with 2000 to 5000 cells/mL per well in serum-free DMEM/F-12 medium (Gibco BRL Life Technologies Inc, USA) supplemented with 20 ng/mL EGF (PeproTech), 4 μg/mL insulin (PeproTech), 20 ng/mL basic FGF (PeproTech) and 0.4% B27 (Invitrogen). During culture, half of medium was replaced every other day with fresh medium. Spheres were counted and imaged 7 d after continuous culture.

2.7. Limiting dilution assay

Briefly, cells were seeded into 96-well ultra-low attachment culture plates (Corning Costar Inc, Corning, NY, USA) with varied cell numbers, followed by treatment with 20 μM of DFCAF and DFO for 7 d. Afterwards, tumor spheres were examined and counted.

2.8. CSC determination by flow cytometry

Original 4T1 cells and cells collected from 4T1 cell-derived mammospheres with or without treatment were incubated with 10% FBS for 30 min, followed by incubation with anti-CD24 and anti-CD44 antibodies (BioLegend) for 20 min at 22 °C in the dark. After washing with PBS for three times, cells were collected and analyzed by flow cytometry.

2.9. ALDH level analysis

After treatment, cells were fixed with 4% methanol for 5 min and thereafter with 0.1% PBS-Tween (Solarbio Science & Technology Co., Ltd., Beijing, China) for 15 min. Then, fixed cells were incubated with 10% FBS for 30 min at 22 °C, followed by incubation with an anti-ALDH antibody (Abcam) for 30 min and afterwards the FITC-conjugated anti-rabbit secondary antibody (Proteintech) for 30 min at 22 °C. Cells were finally collected and analyzed through flow cytometry using the NovoCyte 1040 flow cytometer (ACEA Biosciences Inc., China), as previously reported [19,20].

2.10. Wound-healing assay

Wound-healing assay was performed according to the established method [21]. In brief, cells were seeded at 4.0×10^5 cells/well in 6-well plates, and were cultured to reach a full confluency. After scraping the cell monolayer, cells were washed off with PBS, and the plates were then treated with DFO and DFCAF at 20 μM. Plates were imaged after 24 h.

2.11. Transwell cellular motility/invasion assay

Transwell chambers equipped with 8 μm pore size (Corning Costar Inc, Corning, NY, USA) were used to determine the cellular motility/invasion ability of 4T1 cancer cells in response to DFCAF relative to DFO. Cells were seeded onto the upper wells with 3×10^4 cells/well, and conditioned medium (phenol red-free RPMI-1640 medium supplemented with 10% FBS and 1% penicillin/streptomycin) was added into the bottom chambers. Cells were then cultured for 16 h upon the treatment with DFO and DFCAF at 20 μM. Finally, transmigrated cells were visualized with 0.1% crystal violet (Solarbio Science & Technology Co., Ltd., Beijing, China) under a microscope (Hamamatsu

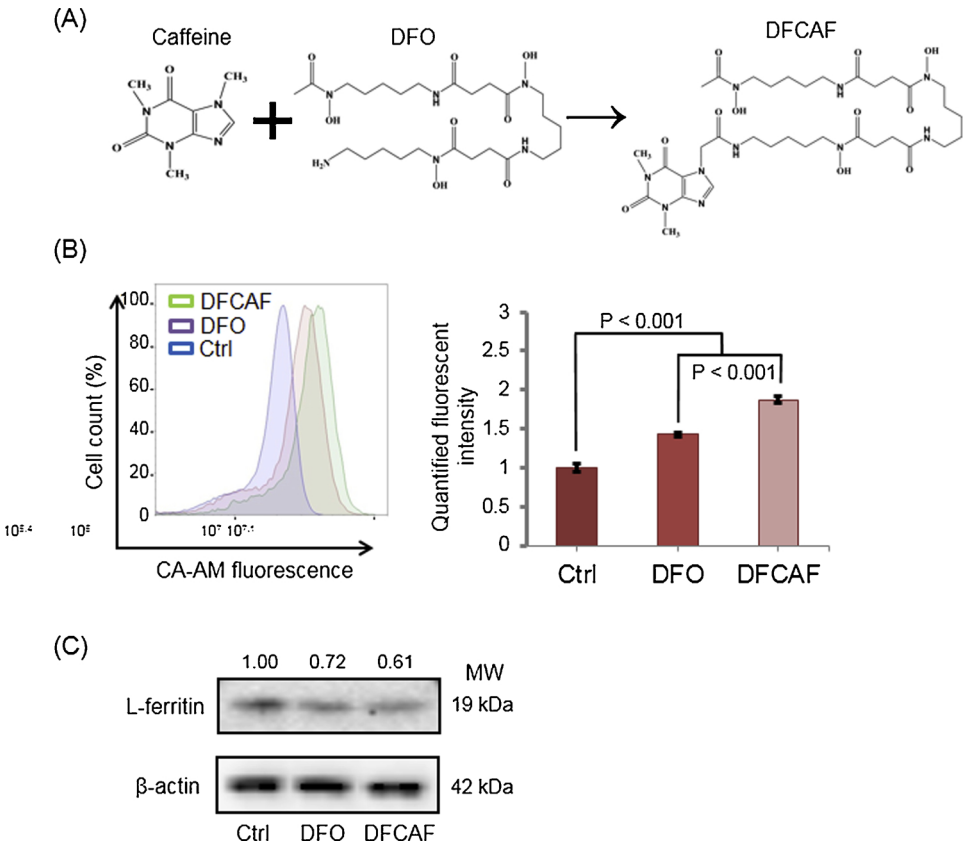

Fig. 1. DFCAF displayed a greater efficacy to chelate iron than DFO.
(A) A scheme delineating the synthesis of DFCAF from DFO and caffeine. (B) The determination of the intracellular iron concentration with the calcein-AM probe. The 4T1 cancer cells were treated with 20 μM of DFO and DFCAF for 24 h, respectively, and calcein-AM fluorescent intensity was determined through flow cytometry. Quantified data were shown in the right panel (n = 3). (C) Protein concentration of ferritin light chain (L-ferritin) was assessed through Western blot analysis in 4T1 cells upon DFO and DFCAF at 20 μM for 24 h.

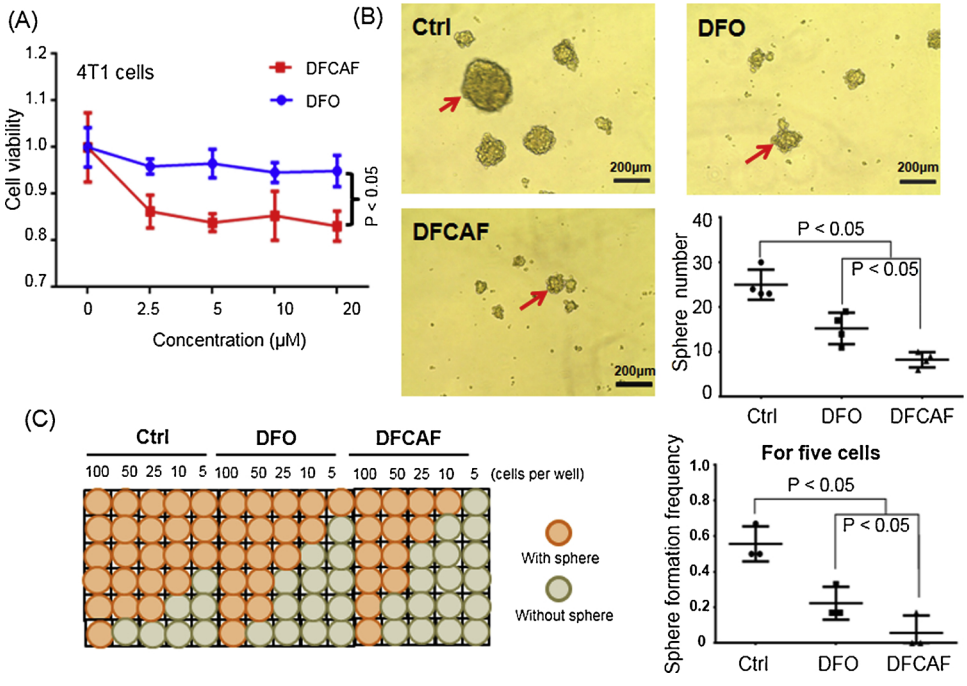

Fig. 2. DFCAF manifested a greater capability to suppress cell viability and sphere formation.
(A) Cell viability evaluation of 4T1 cells responding to DFO and DFCAF at various concentrations for 24 h through CCK8 assay. (B) Sphere formation assay of 4T1 cells upon treatment with 20 μM DFO and DFCAF in 6-well plates for 7 d. Quantified data (n = 4) for sphere numbers per plate were shown in the bottom right corner. (C) Capability of sphere formation from single cell for 4T1 cells in response to 20 μM DFO and DFCAF in 96-well plates for 7 d. Representative 96-well plates harboring mammoshperes in each well. Quantified data (5 cells per well) of three independent experiments were shown in the right panel.

Photonics Co., Ltd., China).

2.12. Statistical analysis

The Independent *t*-test and One-Way ANOVA test were used to analyze the experimental data. Data were presented in mean ± SD. Here, $P < 0.05$ was considered statistically significant.

3. Results and discussion

3.1. DFCAF displayed a greater capability in chelating intracellular iron

To overcome the inherent drawbacks of DFO including limited cellular permeability and low efficiency in targeting cancer cells [22], we here synthesized DFCAF for iron chelation by incorporating caffeine into DFO molecule (Fig. 1A), according to our previous study [12].

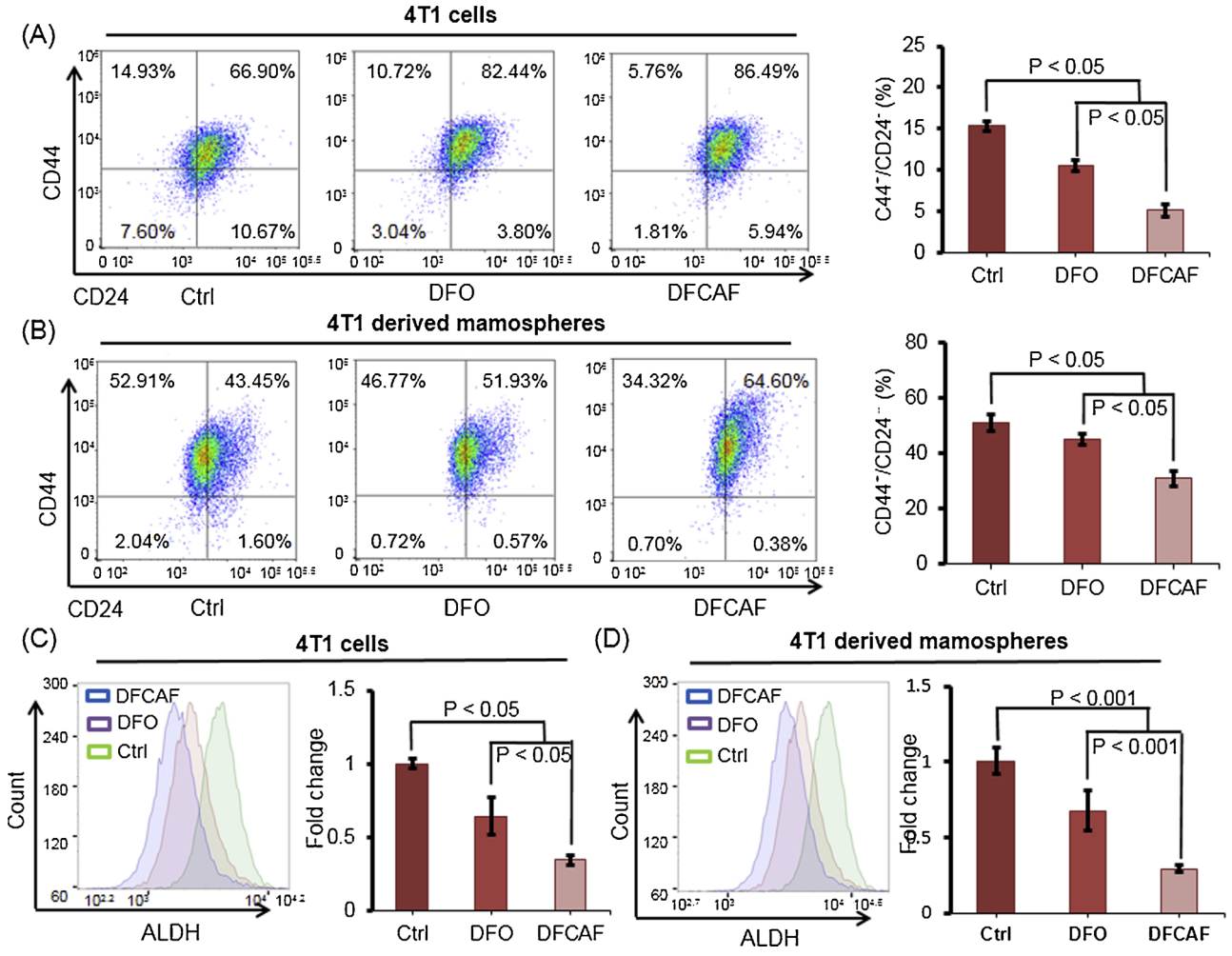

Fig. 3. DFCAF showed a greater ability to deplete CSCs than DFO.
(A) Percentage of $CD44^+/CD24^-$ subpopulation of 4T1 cells responding to DFO and DFCAF at 20 μM for 24 h. Quantified data were presented in the right panel (n = 3). (B) Proportion of $CD44^+/CD24^-$ subpopulation in 4T1-derived spheres responding to 20 μM DFO and DFCAF for 7 d (n = 3). Relative expression of ALDH, as characterized by mean fluorescent intensity in 4T1 cells (C) and 4T1-derived mammospheres (D) treated with 20 μM DFO and DFCAF for 24 h.

First, the iron binding efficacy of DFCAF was determined through flow cytometry analysis using the calcein-AM probe, which manifests a greater green-fluorescent intensity upon the reduction of intracellular iron and reflects the efficacy of iron chelation. After DFO treatment, the fluorescent intensity of intracellular calcein-AM was significantly increased by 43% in 4T1 cells compared to the untreated cells (Fig. 1B and S4, $P < 0.001$). By contrast, DFCAF further depleted the intracellular iron level relative to DFO-treated cells, as demonstrated by 80% elevation of fluorescent intensity in cells upon calcein-AM in comparison to untreated cells (Fig. 1B and S4, $P < 0.001$). To corroborate these findings, we looked into the intracellular iron mass through the level of L-ferritin, which is a key subunit of iron storage protein [23]. Similarly, the protein level of L-ferritin was decreased by 28% in 4T1 cells upon DFO treatment compared to untreated cells, and further declined by 39% in DFCAF-treated cells (Fig. 1C). These data thus suggested a more potent capability of DFCAF in chelating intracellular iron than DFO.

3.2. DFCAF inhibited cell viability and sphere formation of cancer cells

As iron supply is essential for cell growth and survival through a number of intertwined cellular processes including DNA replication, electron transfer, respiration, and enzyme activities [24–26], cell viability was assessed in 4T1 cells upon treatment of DFCAF and DFO. As shown in Fig. 2A, DFO impeded cell viability in a dose-dependent manner with a max inhibition of 9% in comparison to untreated cells, consistent with previous reports [12]. Strikingly, to a greater extent, DFCAF suppressed cell viability in a dose-dependent manner at the same concentrations with a max inhibition of 19% relative to untreated cells (Fig. 2A, $P < 0.05$). Afterwards, we determined the capability of sphere formation, a fundamental characteristic of tumorigenicity following a standard protocol as previously described [27]. As delineated in Fig. 2B, tumorspheres with typical morphological characteristics, *e.g.* solid and round structures with varied size, were formed from 4T1 cells. However, the formation of tumor spheres was inhibited by DFO, and further inhibited by DFCAF, as evidenced by 37% and 63% reduction of sphere numbers per well, respectively (Fig. 2B, $P < 0.05$). Moreover, the average sphere size also showed 38% and 59% reduction for cells treated with DFO and DFCAF, respectively, compared to untreated cells (Fig. S5, $P < 0.001$). To substantiate this finding, we used another strategy to determine sphere formation, limiting dilution assay in 96-well plates [28,29]. In accordance to the above results, the frequency of sphere formation was greatly repressed by DFO and DFCAF in wells starting with all numbers of cells except with 100 cells, as illustrated by the 96-well layout and quantified data (Fig. 2C). For example, the frequency of sphere formation was suppressed by 33% and 50% for the wells with 5 cells upon DFO and DFCAF treatment, compared to the according control without treatment, respectively (Fig. 2C, $P < 0.05$). These results thus revealed more potent inhibition of DFCAF on sphere formation than DFO, and also implied greater cellular permeability of

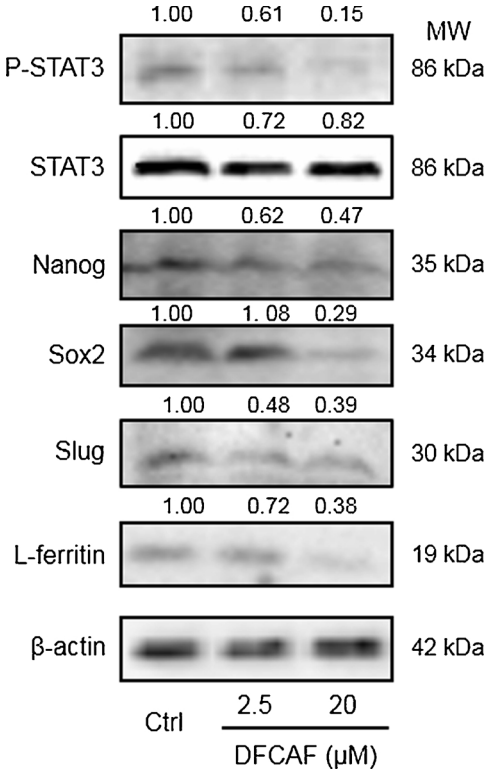

Fig. 4. DFCAF repressed the expression of CSC markers.
Protein amount of STAT3, phosphorylated-STAT3 (P-STAT3), Slug, Sox2, Nanog and ferritin light chain (L-ferritin) in 4T1 cancer cells treated with DFCAF at 2.5 and 20 μM for 24 h through Western blotting. β-actin served as a loading control.

DFCAF than DFO.

3.3. DFCAF diminished the subpopulation of CSCs

Next, we investigated the potential impact of DFCAF on the pool of the CSC subpopulation, which is thought to be the driving force of tumor progression, metastasis, relapse and chemoresistance [30–32]. It has been reported that the relative mass of CSCs can be represented by $CD44^{+/high}/CD24^{-/low}$ subpopulation and $ALDH^{+/high}$ cells [33–35]. As shown in Fig. 3A, DFO repressed the proportion of $CD44^{+/high}/CD24^{-/low}$ subpopulation from 15% in untreated 4T1 cells to 11% ($P < 0.05$). Importantly, DFCAF depleted the proportion of $CD44^{+/high}/CD24^{-/low}$ subpopulation to 6% ($P < 0.05$). Furthermore, we examined the proportion alterations of $CD44^{+/high}/CD24^{-/low}$ subpopulation in mammospheres. Consistent with previous findings [36], significantly enriched $CD44^{+/high}/CD24^{-/low}$ cells were defined in 4T1 cell-derived mammospheres compared to parental 4T1 cells (53% vs 15%, $P < 0.001$) (Fig. 3A and B). Furthermore, DFCAF diminished $CD44^{+/high}/CD24^{-/low}$ cells more dramatically than DFO (19% vs 6%, $P < 0.05$), relative to untreated cells (Fig. 3B).

To substantiate these data on the changes of $CD44^{+/high}/CD24^{-/low}$ subpopulation, the percentage of $ALDH^{+/high}$ cells was further examined [37,38]. The mean fluorescent intensity of ALDH in 4T1 cells was measured by flow cytology (Fig. S6A). As shown in Fig. 3C, the percentage of $ALDH^{+/high}$ cells was greatly reduced by 45% and 60% in parental 4T1 cells upon DFO and DFCAF treatments, respectively, compared to untreated cells ($P < 0.05$). Meanwhile, we observed greater reduction of $ALDH^{+/high}$ cells by DFCAF than DFO in 4T1 cell-derived mammospheres (Fig. 3D and S6B, $P < 0.001$), confirming the greater capability of DFCAF to deplete CSCs.

Thus far, a few markers have been proposed to recognize CSCs, including phosphorylated STAT3 (P-STAT3) [39], Nanog [40], Sox2 [41] and Slug [42]. Subjected to the reduction of intracellular iron mass in cells upon DFCAF at 2.5 and 20 μM, as reflected by the decrease of L-ferritin, the CSC markers, namely P-STAT3, Nanog, Sox2 and Slug, were remarkably compromised in cells treated with DFCAF, especially at 20 μM (Fig. 4). To this end, these results together supported the rationale of iron chelation to diminish CSC subpopulation. Our data also demonstrated a more potent capability of DFCAF to diminish CSC subpopulation than DFO, suggesting a greater efficacy of DFCAF for targeting CSCs.

3.4. DFCAF restrained cancer cell motility and invasion

Given that CSCs are believed to the driving force of tumor metastasis and epithelial-mesenchymal transition (EMT) [43], we next investigated the influence of DFCAF treatment on cancer cell motility, invasion and EMT. As shown in Fig. 5A, DFO and DFCAF inhibited cell mobility of 4T1 cells by 47% and 71%, compared to untreated cells ($P < 0.05$), respectively, as demonstrated by the wound-healing assay. In support of this finding, cell motility/invasion of 4T1 cells was repressed by 44% and 68% by DFO and DFCAF, respectively, compared to untreated cells (Fig. 5B, $P < 0.05$), as characterized by the transwell assay. The capability of cellular motility/invasion is closely dictated by the EMT properties of cancer cells [44–46]. Thereafter, we embarked on the alterations of EMT markers in 4T1 cells upon DFCAF treatment. As shown in Fig. 5C, an increased level of an epithelial marker, E-cadherin, and reversely a decreased level of a mesenchymal marker, N-cadherin, were found in 4T1 cells upon DFCAF treatment, especially at 20 μM (Fig. 5C). These data thus suggested largely compromised EMT for 4T1 cells responding to DFCAF, accounting for reduced cellular motility and invasion, as observed above. Collectively, our data revealed a potent efficacy of DFCAF in inhibiting cell motility/invasion and EMT.

4. Conclusions

To summarize, our combined data uncovered a greater capability of the DFO derivative, DFCAF, to chelate intracellular iron with a greater efficacy than DFO. DFCAF showed much better performance in suppressing cell growth and restraining cellular mobility/invasion than DFO. Moreover, DFCAF was uncovered to remarkably deplete CSC subpopulation and to reverse EMT, which has not been recognized through the strategy of iron chelation in the past. Together, our data unveiled enhanced cellular permeability of DFACF to target cancer cells and even CSCs, resulting in compromised cell growth, cellular motility/invasion and EMT.

Conflicts of interest statement

None declared.

Acknowledgments

This research was supported by the Strategic Priority Research Program of the Chinese Academy of Sciences (Grant No. XDB14000000), grants from the National Natural Science Foundation of China (Grant No.: 21425731 and 21637004) and the national “973” program (Grant No. 2014CB932000). The authors thanks Mr Jesus Huayhuaz and Drs Dibakar Goswami, M. Terêsa Machini and Cleber Liria for their technical support.

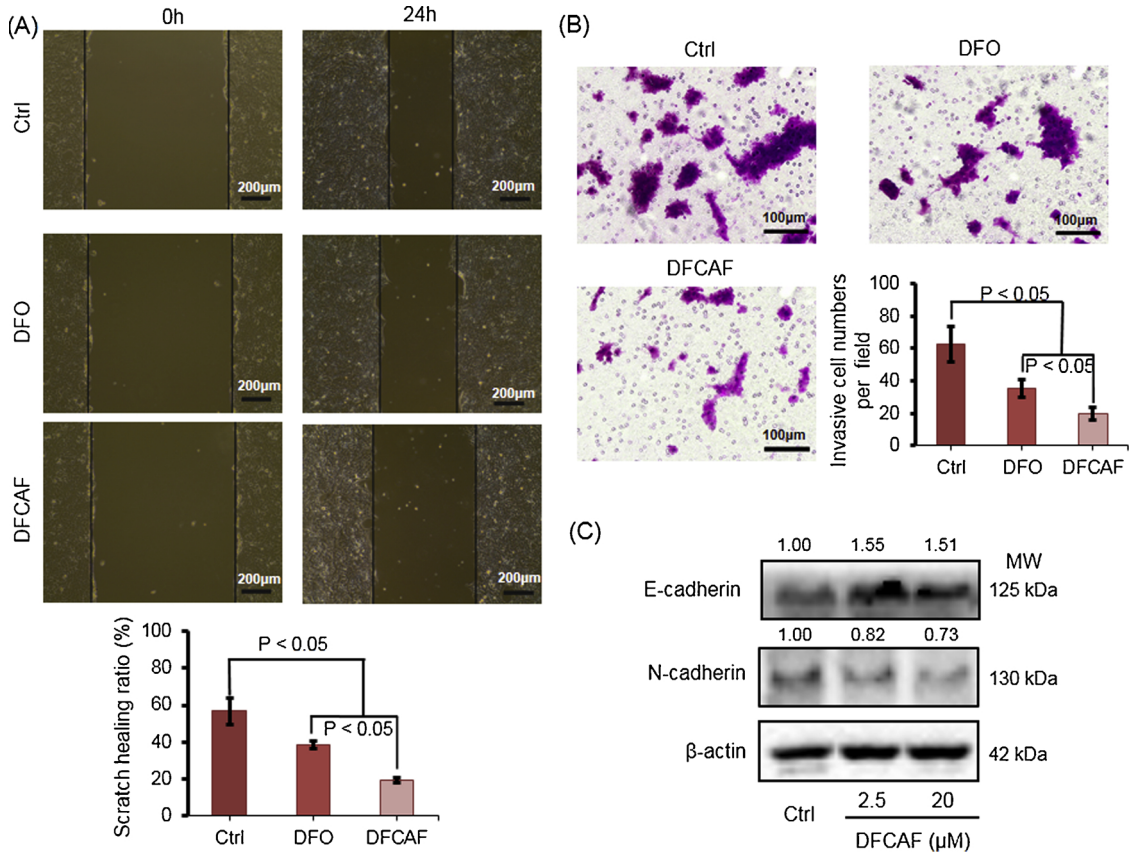

Fig. 5. DFCAF repressed cellular migration and motility.
(A) The cellular motility was assessed through the wound-healing assay. The wound area was indicted between dash lines in each image. The bottom panel presented the healing/scratching ratio for 4T1 cells upon DFO and DFCAF at 20 μM for 2 h (n = 3). (B) The invasion/migration ability assessment of 4T1 cells upon DFO and DFCAF at 20 μM for 16 h through the transwell assay. Transmigrated cells were visualized through crystal violet staining. Quantified data were shown in the bottom right corner (n = 3). (C) Protein levels of E-cadherin and N-cadherin in 4T1 cells treated with DFCAF at 2.5 and 20 μM for 24 h through Western blot analysis.

Appendix A. Supplementary data

Supplementary material related to this article can be found, in the online version, at doi:https://doi.org/10.1016/j.jtemb.2019.01.004.

References

[1] L. Zhou, B. Zhao, L. Zhang, S. Wang, D. Dong, H. Lv, P. Shang, Alterations in cellular Iron metabolism provide more therapeutic opportunities for cancer, Int. J. Mol. Sci. 19 (5) (2018).

[2] S. Puig, L. Ramos-Alonso, A.M. Romero, M.T. Martinez-Pastor, The elemental role of iron in DNA synthesis and repair, Metall.: Integr. Biomet. Sci. 9 (11) (2017) 1483–1500.

[3] D. Vela, Z. Vela-Gaxha, Differential regulation of hepcidin in cancer and non-cancer tissues and its clinical implications, Exp. Mol. Med. 50 (2) (2018) e436.

[4] D. Basuli, L. Tesfay, Z. Deng, B. Paul, Y. Yamamoto, G. Ning, W. Xian, F. McKeon, M. Lynch, C.P. Crum, et al., Iron addiction: a novel therapeutic target in ovarian cancer, Oncogene 36 (29) (2017) 4089–4099.

[5] H.H. Kazan, C. Urfali-Mamatoglu, U. Gunduz, Iron metabolism and drug resistance in cancer, Biomet.: Int. J. Role Met. Ions Biol. Biochem. Med. 30 (5) (2017) 629–641.

[6] H. Padmanabhan, M.J. Brookes, T. Iqbal, Iron and colorectal cancer: evidence from in vitro and animal studies, Nutr. Rev. 73 (5) (2015) 308–317.

[7] M.J. Kerins, A. Ooi, The roles of NRF2 in modulating cellular Iron homeostasis, Antioxid. Redox Signal. (2017), https://doi.org/10.1089/ars.2017.7176.

[8] M. Inoue-Choi, R. Sinha, G.L. Gierach, M.H. Ward, Red and processed meat, nitrite, and heme iron intakes and postmenopausal breast cancer risk in the NIH-AARP Diet and Health Study, Int. J. Cancer 138 (7) (2016) 1609–1618.

[9] C. McLeod, N. Fleeman, J. Kirkham, A. Bagust, A. Boland, P. Chu, R. Dickson, Y. Dundar, J. Greenhalgh, B. Modell, et al., Deferasirox for the treatment of iron overload associated with regular blood transfusions (transfusional haemosiderosis) in patients suffering with chronic anaemia: a systematic review and economic evaluation, Health Technol. Assess. (Rockv.) 13 (1) (2009) 1–121 iii-iv, ix-xi.

[10] L. Lan, W. Wei, Y. Zheng, L. Niu, X. Chen, D. Huang, Y. Gao, S. Mo, J. Lu, M. Guo, et al., Deferoxamine suppresses esophageal squamous cell carcinoma cell growth via ERK1/2 mediated mitochondrial dysfunction, Cancer Lett. 432 (2018) 132–143.

[11] P. Heffeter, V.F.S. Pape, E.A. Enyedy, B.K. Keppler, G. Szakacs, C.R. Kowol, Anticancer Thiosemicarbazones: Chemical Properties, Interaction with Iron Metabolism, and Resistance Development, Antioxid. Redox Signal. 10 (2018) 1089.

[12] E.C. Alta, D. Goswami, M.T. Machini, D.M. Silvestre, C.S. Nomura, B.P. Esposito, Desferrioxamine-caffeine (DFCAF) as a cell permeant moderator of the oxidative stress caused by iron overload, Biomet.: Int. J. Role Met. Ions Biol. Biochem. Med. 27 (6) (2014) 1351–1360.

[13] M. Peiris-Pages, U.E. Martinez-Outschoorn, R.G. Pestell, F. Sotgia, M.P. Lisanti, Cancer stem cell metabolism, Breast Cancer Res.: BCR 18 (1) (2016) 55.

[14] M. Fedele, L. Cerchia, G. Chiappetta, The epithelial-to-mesenchymal transition in breast cancer: focus on basal-like carcinomas, Cancers 9 (10) (2017).

[15] S. Rivas, C. Gomez-Oro, I.M. Anton, F. Wandosell, Role of Akt Isoforms Controlling Cancer Stem Cell Survival, Phenotype and Self-Renewal, Biomedicines 6 (1) (2018), https://doi.org/10.3390/biomedicines6010029.

[16] H. Shen, C. Mu, X. Wu, X. Zhou, J. Wolfram, J. Shen, D. Zhang, J. Mai, X. Xia, A.M. Holder, et al., Chemotherapy sensitizes therapy-resistant cells to mild hyperthermia by suppressing heat shock protein 27 expression in triple negative breast cancer, Clin. Cancer Res. (2018), https://doi.org/10.1158/1078-0432.

[17] T.T. Mai, A. Hamai, A. Hienzsch, T. Caneque, S. Muller, J. Wicinski, O. Cabaud, C. Leroy, A. David, V. Acevedo, et al., Salinomycin kills cancer stem cells by sequestering iron in lysosomes, Nat. Chem. 9 (10) (2017) 1025–1033.

[18] M. Gao, M. Chen, C. Li, M. Xu, Y. Liu, M. Cong, N. Sang, S. Liu, Long non-coding RNA MT1DP shunts the cellular defense to cytotoxicity through crosstalk with MT1H and RhoC in cadmium stress, Cell Discov. 4 (5) (2018), https://doi.org/10.1038/s41388-018-0218-z.

[19] J. Zhu, M. Xu, M. Gao, Z. Zhang, Y. Xu, T. Xia, S. Liu, Graphene oxide induced perturbation to plasma membrane and cytoskeletal meshwork sensitize Cancer cells to chemotherapeutic agents, ACS Nano 11 (3) (2017) 2637–2651.

[20] S. Zhang, Y. Chen, W. Guo, L. Yuan, D. Zhang, Y. Xu, E. Nemeth, T. Ganz, S. Liu, Disordered hepcidin-ferroportin signaling promotes breast cancer growth, Cell. Signal. 26 (11) (2014) 2539–2550.

[21] S. Liu, R.H. Goldstein, E.M. Scepansky, M. Rosenblatt, Inhibition of rho-associated kinase signaling prevents breast cancer metastasis to human bone, Cancer Res. 69 (22) (2009) 8742–8751.

[22] N.A. Rossi, I. Mustafa, J.K. Jackson, H.M. Burt, S.A. Horte, M.D. Scott, J.N. Kizhakkedathu, In vitro chelating, cytotoxicity, and blood compatibility of degradable poly(ethylene glycol)-based macromolecular iron chelators,

Biomaterials 30 (4) (2009) 638–648.
[23] U. Carmona, L. Li, L. Zhang, M. Knez, Ferritin light-chain subunits: key elements for the electron transfer across the protein cage, Chem. Commun. 50 (97) (2014) 15358–15361.
[24] J.O. Fuss, C.L. Tsai, J.P. Ishida, J.A. Tainer, Emerging critical roles of Fe-S clusters in DNA replication and repair, Biochim. Biophys. Acta 1853 (6) (2015) 1253–1271.
[25] M. Jodeiri Farshbaf, K. Ghaedi, Does any drug to treat cancer target mTOR and iron hemostasis in neurodegenerative disorders? Biomet.: Int. J. Role Met. Ions Biol. Biochem. Med. 30 (1) (2017) 1–16.
[26] J.L. Heath, J.M. Weiss, C.P. Lavau, D.S. Wechsler, Iron deprivation in cancer–potential therapeutic implications, Nutrients 5 (8) (2013) 2836–2859.
[27] M.R. Abbaszadegan, V. Bagheri, M.S. Razavi, A.A. Momtazi, A. Sahebkar, M. Gholamin, Isolation, identification, and characterization of cancer stem cells: a review, J. Cell. Physiol. 232 (8) (2017) 2008–2018.
[28] D. Xiang, Z. Cheng, H. Liu, X. Wang, T. Han, W. Sun, X. Li, W. Yang, C. Chen, M. Xia, et al., Shp2 promotes liver cancer stem cell expansion by augmenting beta-catenin signaling and predicts chemotherapeutic response of patients, Hepatology 65 (5) (2017) 1566–1580.
[29] R. Fedr, Z. Pernicova, E. Slabakova, N. Strakova, J. Bouchal, M. Grepl, A. Kozubik, K. Soucek, Automatic cell cloning assay for determining the clonogenic capacity of cancer and cancer stem-like cells, Cytometry Part A: J. Int. Soc. Analyt. Cytol. 83 (5) (2013) 472–482.
[30] A.Z. Ayob, T.S. Ramasamy, Cancer stem cells as key drivers of tumour progression, J. Biomed. Sci. 25 (1) (2018) 20.
[31] T. Shibue, R.A. Weinberg, EMT, CSCs, and drug resistance: the mechanistic link and clinical implications, Nat. Rev. Clin. Oncol. 14 (10) (2017) 611–629.
[32] C. Zhang, P. Li, Y. Wen, G. Feng, Y. Liu, Y. Zhang, Y. Xu, Z. Zhang, The promotion on cell growth of androgen-dependent prostate cancer by antimony via mimicking androgen activity, Toxicol. Lett. 288 (2018) 136–142.
[33] W.A. Woodward, E.P. Sulman, Cancer stem cells: markers or biomarkers? Cancer Metastasis Rev. 27 (3) (2008) 459–470.
[34] S. Badve, H. Nakshatri, Breast-cancer stem cells—beyond semantics, Lancet Oncol. 13 (1) (2012) e43–e48.
[35] X. Xu, S. Chai, P. Wang, C. Zhang, Y. Yang, Y. Yang, K. Wang, Aldehyde dehydrogenases and cancer stem cells, Cancer Lett. 369 (1) (2015) 50–57.
[36] I.G. Ryoo, B.H. Choi, S.K. Ku, M.K. Kwak, High CD44 expression mediates p62-associated NFE2L2/NRF2 activation in breast cancer stem cell-like cells: implications for cancer stem cell resistance, Redox Biol. 17 (2018) 246–258.
[37] S.-M. Yang, N.J. Martinez, A. Yasgar, C. Danchik, C. Johansson, Y. Wang, B. Baljinnyam, A.Q. Wang, X. Xu, P. Shah, et al., Discovery of Orally Bioavailable, Quinoline-Based Aldehyde Dehydrogenase 1A1 (ALDH1A1) Inhibitors with Potent Cellular Activity, J. Med. Chem. 61 (11) (2018) 4883–4903.
[38] L. Castiello, P. Sestili, G. Schiavoni, R. Dattilo, D.M. Monque, F. Ciaffoni, M. Iezzi, A. Lamolinara, A. Sistigu, F. Moschella, et al., Disruption of IFN-I Signaling Promotes HER2/Neu Tumor Progression and Breast Cancer Stem Cells, Cancer Immunol. Res. 6 (6) (2018) 658–670.
[39] A.R. Ozes, N. Pulliam, M.G. Ertosun, O. Yilmaz, J. Tang, E. Copuroglu, D. Matei, O.N. Ozes, K.P. Nephew, Protein kinase A-mediated phosphorylation regulates STAT3 activation and oncogenic EZH2 activity, Oncogene 37 (26) (2018) 3589–3600.
[40] P.S. Thiagarajan, M. Sinyuk, S.M. Turaga, E.E. Mulkearns-Hubert, J.S. Hale, V. Rao, A. Demelash, C. Saygin, A. China, T.J. Alban, et al., Cx26 drives self-renewal in triple-negative breast cancer via interaction with NANOG and focal adhesion kinase, Nat. Commun. 9 (1) (2018) 578.
[41] H. Bulstrode, E. Johnstone, M.A. Marques-Torrejon, K.M. Ferguson, R.B. Bressan, C. Blin, V. Grant, S. Gogolok, E. Gangoso, S. Gagrica, et al., Elevated FOXG1 and SOX2 in glioblastoma enforces neural stem cell identity through transcriptional control of cell cycle and epigenetic regulators, Genes Dev. 31 (8) (2017) 757–773.
[42] Z. Zhang, P. Zhu, Y. Zhou, Y. Sheng, Y. Hong, D. Xiang, Z. Qian, J. Mosenson, W.S. Wu, A novel slug-containing negative-feedback loop regulates SCF/c-Kit-mediated hematopoietic stem cell self-renewal, Leukemia 31 (2) (2017) 403–413.
[43] M. Singh, N. Yelle, C. Venugopal, S.K. Singh, EMT: mechanisms and therapeutic implications, Pharmacol. Ther. 182 (2018) 80–94.
[44] M.J. Kim, J. Lim, Y. Yang, M.S. Lee, J.S. Lim, N-myc downstream-regulated gene 2 (NDRG2) suppresses the epithelial-mesenchymal transition (EMT) in breast cancer cells via STAT3/Snail signaling, Cancer Lett. 354 (1) (2014) 33–42.
[45] T.R. Sarkar, V.L. Battula, S.J. Werden, G.V. Vijay, E.Q. Ramirez-Pena, J.H. Taube, J.T. Chang, N. Miura, W. Porter, N. Sphyris, et al., GD3 synthase regulates epithelial-mesenchymal transition and metastasis in breast cancer, Oncogene 34 (23) (2015) 2958–2967.
[46] J.M. Hsu, W. Xia, Y.H. Hsu, L.C. Chan, Cha J.H. Yu WH, C.T. Chen, H.W. Liao, C.W. Kuo, K.H. Khoo, et al., STT3-dependent PD-L1 accumulation on cancer stem cells promotes immune evasion, Nat. Commun. 9 (1) (2018) 1908.